

Hydrodynamic attraction and repulsion between asymmetric rotors

This article has been downloaded from IOPscience. Please scroll down to see the full text article.

2010 New J. Phys. 12 073017

(<http://iopscience.iop.org/1367-2630/12/7/073017>)

View [the table of contents for this issue](#), or go to the [journal homepage](#) for more

Download details:

IP Address: 132.180.92.65

The article was downloaded on 22/07/2010 at 08:27

Please note that [terms and conditions apply](#).

Hydrodynamic attraction and repulsion between asymmetric rotors

Steffen Schreiber¹, Thomas Fischer² and Walter Zimmermann^{1,3}

¹ Theoretische Physik I, Universität Bayreuth, D-95440 Bayreuth, Germany

² Experimentalphysik V, Universität Bayreuth, D-95440 Bayreuth, Germany

E-mail: walter.zimmermann@uni-bayreuth.de

New Journal of Physics **12** (2010) 073017 (15pp)

Received 5 February 2010

Published 21 July 2010

Online at <http://www.njp.org/>

doi:10.1088/1367-2630/12/7/073017

Abstract. At low Reynolds numbers, the hydrodynamic interaction between dumbbells driven by an external rotating field can be attractive or repulsive. Dumbbells of dissimilar asymmetric shape or different coupling to the external field undergo conformational rearrangements that break the time-reversal symmetry. The parameter ranges leading to attraction or repulsion are explored numerically. The results of our simulations suggest that rotating fields may be a useful avenue for the assembly, disassembly and sorting of particles of different shapes, as well as for the study of collective micro-swimmers.

Contents

1. Introduction	2
2. Model	3
3. Dumbbell dynamics	4
3.1. Single dumbbell	4
3.2. Two dumbbells	5
4. Conclusions and discussion	14
Acknowledgments	14
References	15

³ Author to whom any correspondence should be addressed.

1. Introduction

Suspensions of active or externally driven nanoparticles or micro-organisms are involved in collective, biological, chemical and technical motion [1]–[9] of fascinating complexity. The propulsion of micro-particles and micro-organisms differs substantially from the motion of macroscopic objects like fish or birds due to the small scale motion at low Reynolds numbers [2]. As a consequence, swimming macro- and micro-organisms transform chemical into translational or rotational energy in different ways. Considerable progress has been made in understanding the propulsion of micro-organisms by studying artificial active swimmers [9]–[12] or active rotors [13]. Self-organization phenomena of assemblies of micro-swimmers can teach us how their interactions via the fluid, the so-called hydrodynamic interactions, synchronize the motion of swimmers or cilia. The importance of hydrodynamic interactions at small Reynolds numbers has been emphasized by showing that by an interplay with deformations they may cause a lift force on vesicles during their motion close to a wall [14]–[16]. They also lead to interesting time-dependent phenomena [17, 18] and cross-streamline migration of droplets, vesicles and deformable bead-spring models in Poiseuille flow [19]–[21]. Additionally, the interplay between Brownian motion of small particles and hydrodynamic interactions can cause surprising anti-correlations and cross-correlations [22, 23].

Macroscopic rotors experience the attractive Magnus force that can easily be understood using the concept of dynamic pressure. The balance of repulsive hydrodynamic forces and attractive magnetic forces can give rise to dynamic, self-assembled structures [7, 24]. These macroscopic hydrodynamic forces scale with the Reynolds number and thus vanish in the Stokes limit [6]. The dynamic self-assembly of small scale rotors is therefore less obvious [25]. Magnetic dipole–hexapole interactions may be used for separating rotors with respect to their shape [26]. Rotors also play an important role in bacterial motion, such as the propulsion of *Escherichia coli* [3] with its rotating flagella. The dynamics of single flagella has recently been modeled in numerical calculations [27]. One fundamental problem for active and driven low Reynolds number motion is the understanding of the influence of hydrodynamic interactions on the collective motion of an assembly of active components.

The aim of this work is to explore the effect of hydrodynamic interactions between two externally driven anisotropic rigid dumbbell rotors (see figure 1). The rotation of these objects is driven by a torque exerted due to a coupling of the dumbbells to a rotating external field. In the case of two identically shaped objects with identical couplings to the external field, symmetry considerations, as described in detail in section 3.2.1, forbid a net change of the system's conformation over one rotational period.

One major question explored here is how to induce attractive or repulsive interactions between the rotors. As the relevant control parameters, we found the difference between the shapes of the rotors and the difference between their couplings to the external field. For these parameters we identified ranges for attractive or repulsive interactions between the rotors.

We demonstrate by numerical calculations that for dissimilar dumbbell shapes and different couplings to the external field the time-reversal symmetry is broken. This broken symmetry is the origin of the attraction and the repulsion between the dumbbells. Transitions between these two effects are induced by changing the torques or the dumbbell shapes. Phase diagrams separating regimes of attraction from regions of repulsion between the dumbbells are constructed for several generic sets of parameters.

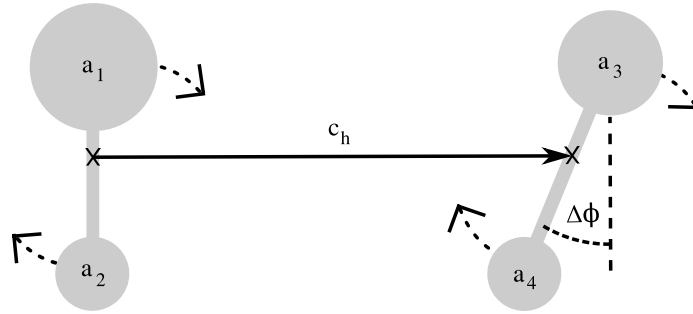


Figure 1. Sketch of two dumbbells with unequal asymmetries, $a_1 \neq a_3$ and $a_2 = a_4$. The dumbbells are rotated by a driving field $\mathbf{f}(t)$, see equation (5). $\Delta\phi$ is the angle between the axes $\hat{\mathbf{r}}_{21}$ and $\hat{\mathbf{r}}_{43}$ of the dumbbells. The crosses indicate the hydrodynamic centers \mathbf{c}_{21} and \mathbf{c}_{43} of the two dumbbells. The distance between them is denoted by c_h .

Our suggestion is to test our theoretical exploration with experiments on anisotropic birefringent particles. Such particles may be rotated by circularly polarized light [28, 29]. Another possibility to apply a torque is to place paramagnetic or ferromagnetic particles in a rotating magnetic field. As in nuclear magnetic resonance, magic angle spinning [30] may be used to eliminate time averaged dipole–dipole interactions that might overshadow the hydrodynamic attraction or repulsion.

2. Model

We investigate the motion of a single dumbbell and of two hydrodynamically interacting dumbbells in a fluid of viscosity η in the low Reynolds number limit. Due to a torque created by a rotating external field \mathbf{f} the dumbbells perform a planar rotational motion. Each dumbbell is composed of two beads that are connected by a bar of constant length, as indicated in figure 1.

The beads with the effective hydrodynamic radii a_i ($i = 1, 2, 3, 4$) at the positions \mathbf{r}_i ($i = 1, 2, 3, 4$) are described as point particles having drag coefficients $\zeta_i = 6\pi\eta a_i$. The vectors $\mathbf{r}_{21} = \mathbf{r}_2 - \mathbf{r}_1$ and $\mathbf{r}_{43} = \mathbf{r}_4 - \mathbf{r}_3$ describe the two dumbbell axes, which we assume to be of constant length $b = |\mathbf{r}_{21}| = |\mathbf{r}_{43}|$. The hydrodynamic centers of the dumbbells, \mathbf{c}_{21} and \mathbf{c}_{43} , are given by

$$\mathbf{c}_{21} = \mathbf{r}_1 + \frac{a_2}{a_1 + a_2} \mathbf{r}_{21} \quad \text{and} \quad \mathbf{c}_{43} = \mathbf{r}_3 + \frac{a_4}{a_3 + a_4} \mathbf{r}_{43}. \quad (1)$$

The equation of the over-damped motion is given by

$$\dot{\mathbf{r}}_i = \mathbf{H}_{ij} \mathbf{F}_j, \quad (2)$$

with the Rotne–Prager mobility matrices for unequal spheres [31, 32]

$$\mathbf{H}_{ij} = \begin{cases} \frac{1}{6\pi\eta a_i} & \text{for } i = j, \\ \frac{1}{8\pi\eta r_{ij}} \left[\left(1 + \frac{1}{3} \frac{a_i^2 + a_j^2}{r_{ij}^2}\right) \mathbf{I} + \left(1 - \frac{a_i^2 + a_j^2}{r_{ij}^2}\right) \hat{\mathbf{r}}_{ij} \otimes \hat{\mathbf{r}}_{ij} \right] & \text{for } i \neq j, \end{cases} \quad (3)$$

the unity matrix \mathbf{I} , the connection unit vectors $\hat{\mathbf{r}}_{ij} = \mathbf{r}_{ij}/|\mathbf{r}_{ij}| = \mathbf{r}_{ij}/r_{ij}$ and the external forces \mathbf{F}_j ($j = 1, 2, 3, 4$) acting on the beads. In our model the rotation of the dumbbells is caused by the potential

$$V = -V_{21} \hat{\mathbf{r}}_{21} \cdot \mathbf{f} - V_{43} \hat{\mathbf{r}}_{43} \cdot \mathbf{f}, \quad (4)$$

with the external field

$$\mathbf{f} = \begin{pmatrix} \cos(\omega t) \\ \sin(\omega t) \end{pmatrix} \quad (5)$$

rotating at a frequency ω in the xy plane and the coupling constants V_{21} and V_{43} between the dumbbell axes and the external field \mathbf{f} . The forces $\mathbf{F}_i = -\nabla_i V$ in equation (2) can be expressed in terms of the rotating field \mathbf{f} as

$$\mathbf{F}_1 = \frac{V_{21}}{r_{21}} [(\hat{\mathbf{r}}_{21} \times \mathbf{f}) \times \hat{\mathbf{r}}_{21}] \quad \text{and} \quad \mathbf{F}_3 = \frac{V_{43}}{r_{43}} [(\hat{\mathbf{r}}_{43} \times \mathbf{f}) \times \hat{\mathbf{r}}_{43}]. \quad (6)$$

The potential in equation (4) yields the following asymmetric relations between the forces: $\mathbf{F}_1 = -\nabla_1 V = \nabla_2 V = -\mathbf{F}_2$ and $\mathbf{F}_3 = -\nabla_3 V = \nabla_4 V = -\mathbf{F}_4$. According to this property, together with equation (6), the dumbbells are force free. Additionally, the forces acting on the individual beads are perpendicular to the dumbbell axes, which results in a rotation of the dumbbells.

The form of the potential V for the driving field is similar to that of magnetic dipoles in an external magnetic field where the interaction between the dipoles is neglected. But other means to propel the dumbbells are possible. For example, non-spherical birefringent particles can be rotated by circularly polarized light. The magnitude of the torques imposed on the dumbbells can easily be tuned by the applied power of the light [28, 29].

3. Dumbbell dynamics

The balance between the driving and the viscous torques leads to phase angles ϕ_{21} and ϕ_{43} between the dumbbell orientations \mathbf{r}_{ij} and the driving field $\mathbf{f}(t)$ with $\cos(\phi_{ij}) = \mathbf{r}_{ij} \cdot \mathbf{f}/|\mathbf{r}_{ij} \cdot \mathbf{f}|$. The dynamics of the dumbbells is analyzed in this section. The conditions under which both dumbbells attract or repel are discussed.

3.1. Single dumbbell

The two beads of a single dumbbell ($V_{43} = 0$ and $V_{21} = V_0$) move on circular trajectories around their hydrodynamic center \mathbf{c}_{21} . The radii $R_{1,2}$ of those trajectories depend on the effective hydrodynamic radii $a_{1,2}$ of the two beads and the length b of the dumbbell axis. In the Oseen approximation they are given by

$$R_1 = \frac{a_2 b}{a_1 + a_2} \quad \text{and} \quad R_2 = \frac{a_1 b}{a_1 + a_2}. \quad (7)$$

For a sufficiently strong external field

$$V_0 > V_{\text{crit}} = \frac{\pi \eta \omega b^2}{\frac{1}{6a_1} + \frac{1}{6a_2} - \frac{1}{4b} \left(1 + \frac{a_1^2 + a_2^2}{3b^2}\right)}. \quad (8)$$

the dumbbell axis \mathbf{r}_{21} rotates synchronously with the driving field $\mathbf{f}(t)$ at the same frequency $\Omega = \omega$. The stationary phase angle ϕ_{21} between the dumbbell axis and the orientation of the external field is given by the expression

$$\sin \phi_{21} = -\frac{\pi \eta \omega b^2}{V_0 \left[\frac{1}{6a_1} + \frac{1}{6a_2} - \frac{1}{4b} \left(1 + \frac{a_1^2 + a_2^2}{3b^2} \right) \right]}. \quad (9)$$

ϕ_{21} tends to zero for decreasing values of the ratio ω/V_0 , i.e. either for a decreasing frequency or for increasing values of the coupling V_0 . If the expression on the right-hand side in equation (9) takes values outside of the interval $[-1, 1]$, the driving torque is too small to enforce a synchronous rotation. These analytical results are in agreement with numerical integrations of equation (2).

3.2. Two dumbbells

In the case of two rotated dumbbells, each experiences the perturbed liquid flow created by the other. Due to this interaction the hydrodynamic centers \mathbf{c}_{ij} are set in motion. In the mean this results in a circular or a spiral-like motion, as indicated in figure 2.

There are two time scales in the system. The typical time corresponding to the rotating external field is $\tau_f = 1/\omega$, whereas the time scale of the dumbbell motion is given by $\tau_d = \eta b^3/V_{ij}$. The dimensionless ratio $\tau_f/\tau_d = V_{ij}/(\eta \omega b^3)$ describes how quickly the dumbbells follow the external field. In order to vary this ratio it is sufficient to change only the coupling V_{ij} and keep the viscosity $\eta = 10$, the dumbbell length $b = 3$ and the angular frequency $\omega = 5 \times 10^{-4}$ fixed. Whether the dumbbells attract or repel depends crucially on the asymmetries a_1/a_2 and a_3/a_4 of the dumbbells, as will be shown later in this work. Therefore, we fix the values $a_2 = a_4 = 1$ and vary the remaining two radii a_1 and a_3 .

The complete conformation of the system (up to a rotation of the whole system) can be described by the distance $D(t)$ between the hydrodynamic centers of the dumbbells,

$$D(t) = |\mathbf{c}_h| = |\mathbf{c}_{21} - \mathbf{c}_{43}| = \left| \mathbf{r}_1 + \frac{a_2}{a_1 + a_2} \mathbf{r}_{21} - \mathbf{r}_3 - \frac{a_4}{a_3 + a_4} \mathbf{r}_{43} \right|, \quad (10)$$

as well as the conformation angles ψ_{21} and ψ_{43} , which are given by

$$\cos(\psi_{ij}) = \frac{\mathbf{c}_h \cdot \mathbf{r}_{ij}}{|\mathbf{c}_h \cdot \mathbf{r}_{ij}|}. \quad (11)$$

The hydrodynamic interactions between the dumbbells induce a slow rotation of \mathbf{c}_h and oscillations of $D(t)$ around some mean distance as indicated by figure 2. The frequency Ω' of these oscillations is the rotation frequency of the dumbbell axes \mathbf{r}_{21} and \mathbf{r}_{43} with respect to \mathbf{c}_h . Therefore, the frequency of the slow rotation of \mathbf{c}_h is equal to the difference $\Omega - \Omega'$.

3.2.1. Two dumbbells having identical shapes and couplings. The dumbbell dynamics is considerably simplified for equally asymmetric shapes of the two dumbbells, $a_1 = a_3$, and equal couplings, $V_{21} = V_{43}$. If the two dumbbells are also equally oriented, as sketched in figure 2(a), the phase angles are equal, $\phi_{21} = \phi_{43} = \phi$, and the conformation angles are identical for all times, $\psi_{21} = \psi_{43} = \psi$. For two oppositely oriented dumbbells the phase difference has the constant value $\Delta\phi = \pi$, whereas the conformation angles add up to $\psi_{21} + \psi_{43} = \pi$.

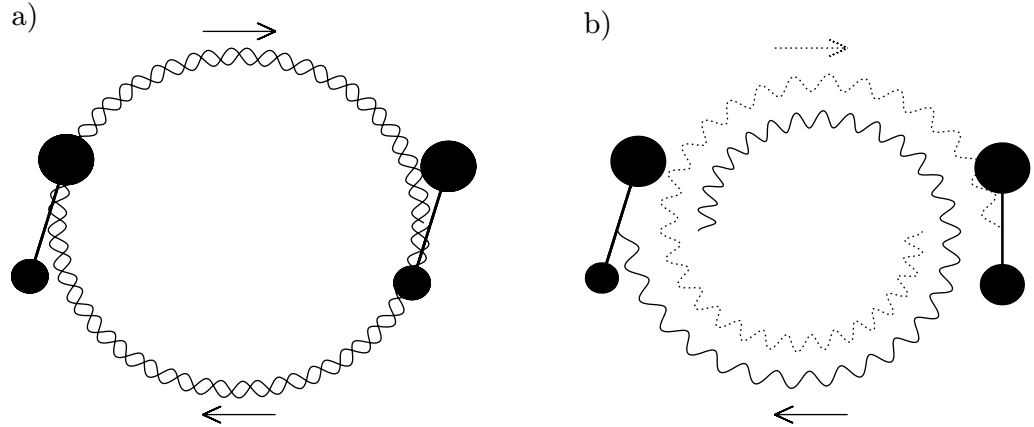


Figure 2. In part (a), the trajectories of the centers of two rotating, equally oriented and equally asymmetrically shaped dumbbells are sketched. In addition to that, the coupling parameters, $V_{21} = V_{43}$, are identical. The trajectories of both hydrodynamic centers \mathbf{c}_{21} and \mathbf{c}_{43} have the same mean radius, which corresponds to the mean length of the vector \mathbf{c}_h . Part (b) corresponds to the case of two dumbbells with differently asymmetric shapes and different coupling strengths ($V_{21} \neq V_{43}$). The resulting trajectories are open and the mean distance $D(t) = |\mathbf{c}_h|$ increases during the motion.

According to the symmetry of the system, the distance $D(t)$ between the hydrodynamic centers of two equally oriented dumbbells oscillates around a mean distance with the frequency $2\Omega'$, as indicated by the sketch in figure 2(a). The corresponding oscillation period is π/Ω' , which is shown for a specific parameter set in figure 3(a). In contrast to this, the distance $D(t)$ for two dumbbells with opposite shape orientation oscillates with a period of $\tau_{\Omega'} = 2\pi/\Omega'$ being twice as long as in the former case. For comparison we show the x -component of the driving field $f_x(t)$ in figure 3(c), which illustrates the inequality of the frequencies, $\Omega' < \Omega$, and thus the inequality of the oscillation periods $\tau_{\Omega'} > \tau_{\Omega} = 2\pi/\Omega$.

In figure 3(b), the oscillatory contribution $\tilde{\psi}$ to the phase $\psi = \Omega't + \tilde{\psi}$ is shown. Since the coupling strengths of the dumbbells are constant, the oscillation of ψ about a linearly growing part confirms that the rotational hydrodynamic drag changes as a function of the relative orientation of the dumbbell axes with respect to \mathbf{c}_h . In the case of equally oriented dumbbells the viscous drag is maximal in the ranges about the conformation angles $\psi = (2n - 1)\pi/4$ ($n = 1, 2, 3, 4$) where fluid between the dumbbells is squeezed out or sucked into the region between the dumbbells. These are also the phases of the rotation during which the repulsion (respectively attraction) between the dumbbells is strongest.

According to the symmetry of the system, the attractive forces acting between the two dumbbells in one quarter of a period ($0 < t < \tau_{\Omega'}/4$) are compensated for during the consecutive quarter ($\tau_{\Omega'}/4 < t < \tau_{\Omega'}/2$) by repulsive forces of the same magnitude. This causes an oscillation of $D(t)$ with the frequency $2\Omega'$ around some mean value, but without a net attraction or repulsion. In the case of oppositely oriented dumbbells, two consecutive maxima of the viscous drag have different amplitudes and therefore the attractive and repulsive hydrodynamic forces do not cancel each other completely during one half of an oscillation period, but during a whole rotation with the period $\tau_{\Omega'}$.

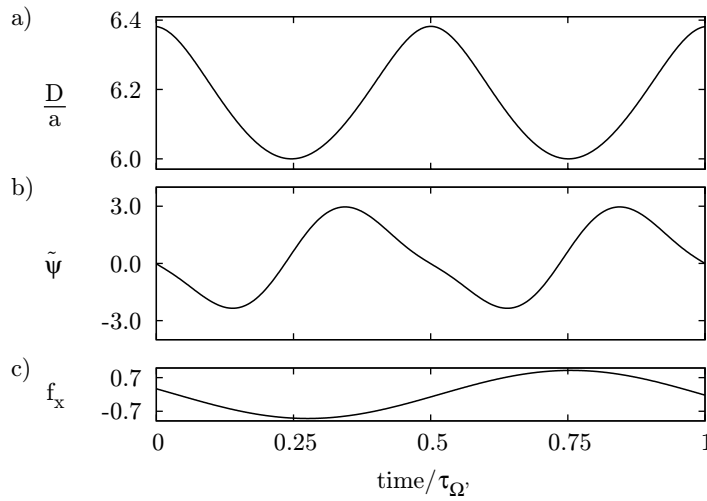


Figure 3. Part (a) shows the dimensionless distance $D(t)/a$ for two equally asymmetrically shaped and equally oriented dumbbells with $a_1 = a_3 = 1.2$ and $V_{21} = V_{43} = 0.7$. In part (b), we present the periodic contribution to the phase angle $\tilde{\psi} = \psi - \Omega't$. For comparison the periodic variation of the x -component of the driving field f is shown in part (c).

During the rotation the viscous drag acting on the inner beads, which are closer to the respective other dumbbell, is higher than the drag on the outer beads of the dumbbells. These differing drag forces induce an oscillation of the phase angles ϕ_{ij} during the rotation.

In the ranges of increasing (decreasing) viscous drag, the rotation frequency Ω' of the dumbbell axes decreases (increases). When Ω' is larger (smaller) than ω , the phase delays ϕ_{ij} of the dumbbells decrease (increase).

The oscillations of $D(t)$ and $\phi(t)$ are shown as a function of time for two different values of the coupling constants in figure 4. In part (a) the coupling to the driving field is weak, $V_{21} = V_{43} = 0.7$, and in part (b) the coupling is strong, $V_{21} = V_{43} = 100$. The amplitudes of the oscillations of the distance are the same in both cases. In contrast to that, the phase lag ϕ of the dumbbell axes with respect to the orientation of the external field is smaller in the case of large values of the coupling. Moreover, the diagrams in figure 4 show that the oscillations of ϕ are in phase with the oscillations of the distance in the case of strong couplings to the external field. Contrary to that, $\phi(t)$ is delayed with respect to $D(t)$ for weak couplings.

The reason for this delay is as follows. While the distance between the dumbbells increases, the drag on the dumbbells also grows. So the rotation frequency Ω' of the dumbbells must decrease. As soon as it is below ω , the phase angle ϕ grows and so does the torque on the dumbbells ($\sim \sin \phi$). But for weak couplings the torque builds up much more slowly than for strong couplings. So for small coupling constants even in the beginning of the domain where the distance (and thus the drag) decreases, ϕ is still growing because the torque is too weak. At some point the torque is large enough to overcome the drag so that ϕ decreases again afterwards. An analogous argument holds in the ranges where $D(t)$ is increasing. The shift between the curves of $D(t)$ and $\phi(t)$ has to be smaller than a quarter of an oscillation period in our considerations because otherwise the field $f(t)$ would be too weak to enforce a synchronous rotation of the dumbbells at all.

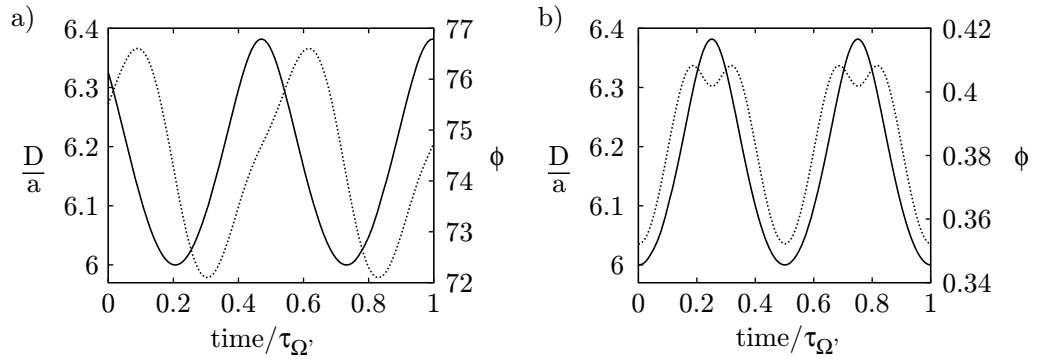


Figure 4. The distance $D(t)$ (solid line) and the phase lag $\phi = \phi_{21} = \phi_{43}$ (dashed line) are shown as a function of time for $a_1 = a_3 = 1.2$. In part (a) the coupling is weak, $V_{21} = V_{43} = 0.7$, and in part (b), the coupling constants are large, $V_{21} = V_{43} = 100$.

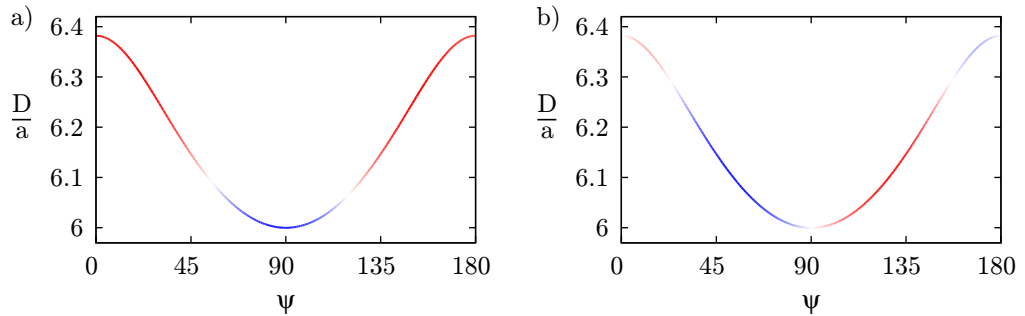


Figure 5. Trajectories in the D - ψ plane for a system of two dumbbells with $a_1 = a_3 = 1.2$ and equal coupling constants. In part (a) the couplings are $V_{12} = V_{34} = 0.7$ and in part (b) $V_{12} = V_{34} = 100$. Both trajectories are invariant under the transformation $\psi \rightarrow -\psi$, showing the reciprocity of the motion. What is more, the trajectories fall on top of each other, which illustrates the universality of the trajectories. However, according to the two different couplings the rates $\dot{\psi}$ along the trajectories differ. The rates $\dot{\psi}$ are color coded, where red denotes a rate below the average, and blue a rate above.

For strong couplings there are small dips at the maxima of $\phi(t)$. These correspond to local minima of the drag, which occur when the dumbbells are aligned with each other so that the four beads lie on a single line. In this conformation the distance between the dumbbells is maximal. An equivalent phenomenon can be seen in the plot of $\phi(t)$ for weak coupling. Of course there is also a local minimum of the drag when the dumbbells are aligned with each other and the distance is maximal. But due to the weak torque acting at that stage there is no dip but only a slight flattening of the curve in this case.

In the coordinate system rotating with the connection vector \mathbf{c}_h the conformation after one period τ_Ω maps on top of the original conformation. The reciprocity of the motion is illustrated in figure 5, where the distance D is plotted as a function of the conformation angle ψ for weak couplings, $V_{12} = V_{34} = 0.7$, in part (a) and strong couplings, $V_{12} = V_{34} = 100$, in part (b).

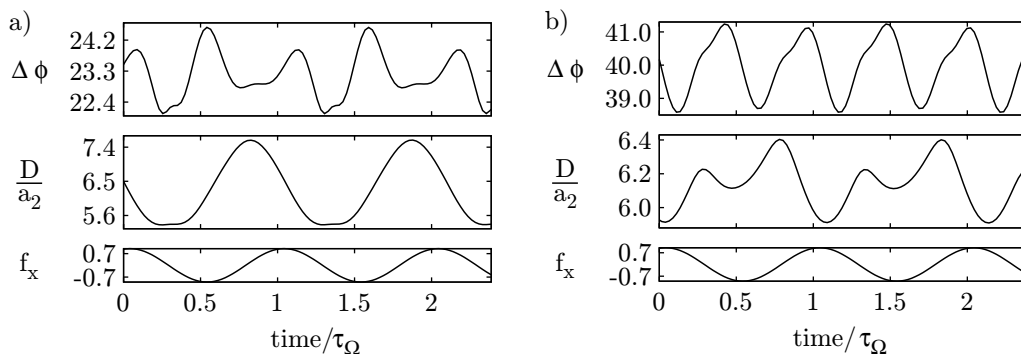


Figure 6. The upper parts show the phase difference $\Delta\phi$ between the two axes of the rotating dumbbells as a function of time. The distance $D(t)$ is plotted in the middle parts and the lower parts show the x -component of the driving field f . In part (a) the two dumbbells repel each other. The corresponding parameters are $a_1 = 1.8$, $a_3 = 0.6$, $V_{21} = 1.2$ and $V_{43} = 1.0$. In part (b) the dumbbells attract each other. There the parameters are $a_1 = 1.2$, $a_3 = 1.1$, $V_{21} = 3.2$ and $V_{43} = 0.8$.

Both curves are invariant under the transformation $\psi \rightarrow -\psi$. This underlines the reciprocity of the motion as it can already be seen in the plot of $D(t)$, which is invariant under time reversal $t \rightarrow -t$. In addition to that, the curves for weak and strong couplings are identical in the conformation space $D-\psi$, as shown in figure 5. In fact the trajectories shown are universal for all values of the coupling constants as long as they are large enough so that the dumbbells can follow the field $f(t)$ synchronously.

However, the rate of change of the conformation angle $\dot{\psi}$ along the curves depends very much on the coupling parameters (see figure 4). This is indicated by the color code along the two curves, where red and blue mark the rates $\dot{\psi}$ below and above the angular frequency Ω' . This shows that irrespective of the strength of the driving field, the dumbbells pass through the same set of conformations during one cycle, although each conformation is passed at a different rate, as indicated by the distribution of the different colors along both lines. The reciprocity of the motion ensures that for a given rotational frequency the distance of the dumbbells described by the Stokesian dynamics is locked to the individual orientation of the dumbbells with respect to \mathbf{e}_h and returns to the same value after one period.

3.2.2. Two dumbbells of dissimilar shapes or couplings. For two differently shaped dumbbells or for different couplings to the external field, the phase difference $\Delta\phi$ and the distance $D(t)$ are plotted as functions of the time in figure 6 for two different sets of parameters. For comparison, the x -component f_x of the driving field is also shown. In contrast to the previous section, the phase difference $\Delta\phi(t)$ oscillates in time. The time dependence is different for different parameters, as indicated in figure 6(a) for the parameters $a_1 = 1.8$, $a_3 = 1.0$, $V_{21} = 1.2$ and $V_{43} = 1.0$, and in figure 6(b) for the parameters $a_1 = 1.2$, $a_3 = 1.1$, $V_{21} = 1.0$ and $V_{43} = 2.0$.

In the previous section, $D(t)$ was oscillating with the frequency $2\Omega'$ or Ω' , but in both cases $D(t)$ was symmetric with respect to a reflection of time (see figure 4). Here, both $D(t)$ and $\Delta\phi(t)$, are not symmetric anymore with respect to time reflection.

As in the case of equally asymmetric dumbbells, the viscous drag is a function of the angles that the dumbbell axes enclose with the vector \mathbf{e}_h . There are also ranges of the phase angles,

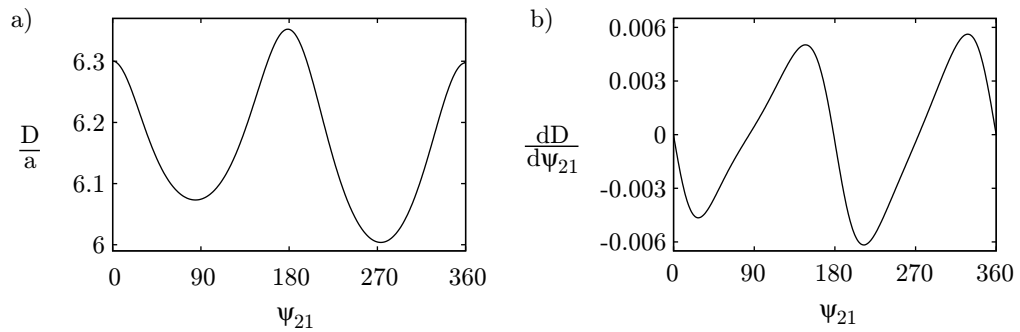


Figure 7. In part (a), the distance $D(t)$ between two dumbbells is plotted as a function of the conformation angle ψ_{21} between the axis of the first dumbbell and the vector \mathbf{c}_h . Part (b) shows the derivative of $D(t)$ as a function of ψ_{21} . The parameters are $a_1 = 1.2$, $a_3 = 1.1$, $V_{21} = 3.2$ and $V_{43} = 0.8$. The dynamics of this system is much more complex than for equally asymmetric dumbbells with equal couplings (see figure 5).

in which liquid is squeezed out between the dumbbells and others where fluid is sucked in. As a consequence, the length of the vector \mathbf{c}_h is also oscillating here, i.e. there are phase ranges of dumbbell attraction, which are followed by phases of dumbbell repulsion and so on.

For finite values of $\Delta\phi \neq 0$, which are a consequence of the broken symmetry, the conformation angles ψ_{21} and ψ_{43} differ from each other. Combined with the hydrodynamic interactions, which depend nonlinearly on the distances between the beads, the magnitude and the directions of the forces between the beads during one rotation cycle are quite complex. Therefore, the trajectories in the configurational space are no longer universal.

For one parameter set the distance $D(t)$ is plotted as a function of the conformation angle ψ_{21} in figure 7(a). It is clear from first sight that the behavior is much more complex here than in the case of equally asymmetric dumbbells with equal couplings, which was shown in figure 5. In particular, the magnitudes of the attraction and repulsion between the dumbbells during the different stages of the motion are different here. So, *a priori*, it is no longer clear whether the dumbbells can attract or repel each other during a whole rotational period. In order to illustrate the complex behavior of D as a function of ψ_{21} in more detail, figure 7(b) shows the derivative $(\partial D / \partial \psi_{21})(\psi_{21})$. In the ranges of the conformation angle ψ_{21} , when this function is positive the dumbbells repel each other and when the function is negative they attract each other. The Fourier modes of this function are given in figure 8. In this spectrum, one can clearly see that there is a non-vanishing coefficient of zeroth order, which means that the distance between the dumbbells changes during a complete dumbbell rotation. But it is also obvious that this net repulsive or attractive effect is superimposed by much stronger oscillations. So it is not possible to determine in which phase of the motion the decisive effect takes place that causes the overall repulsion or attraction. In fact all coefficients from $n = 1$ ($\sim e^{i\psi_{21}}$) to $n = 8$ ($\sim e^{8i\psi_{21}}$) are larger than the zero-order coefficient.

As shown above, the mean distance between two unequally shaped dumbbells may increase, as sketched in figure 2(b), or decrease as a function of time. In figure 9, we have plotted $D(t)$ for the same parameter sets as in figure 6, but for a longer time window. One can easily see that in the mean the dumbbells repel each other in part (a) and attract each other in

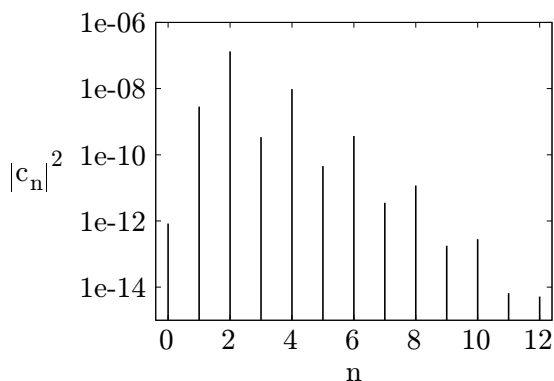


Figure 8. The Fourier modes of the function $(\partial D/\partial \psi_{21})$ are shown. There is a non-vanishing zeroth-order coefficient that leads to an attraction or a repulsion between the dumbbells. However, there are eight higher-order coefficients that have larger values, which indicate a quite complex motion.

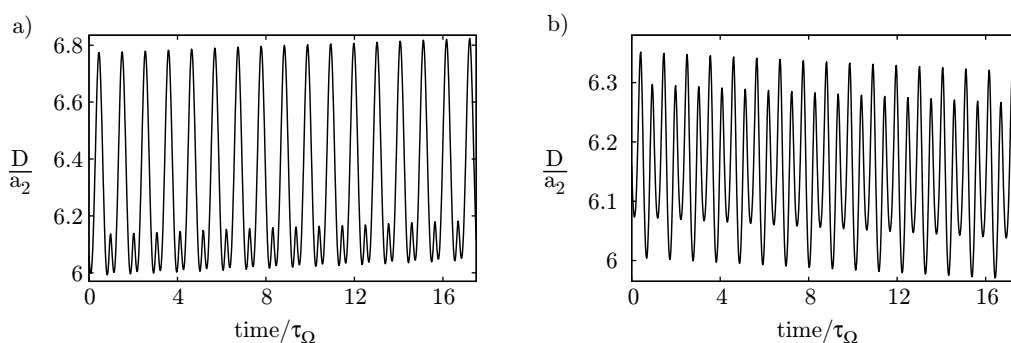


Figure 9. The distance $D(t)$ between the centers of the dumbbell is shown as a function of the time for the same two parameter sets as in figure 6. In part (a) the dumbbells repel each other. The parameters are $a_1 = 1.8$, $a_3 = 0.6$, $V_{21} = 1.2$ and $V_{43} = 1.0$. In part (b) the dumbbells attract each other for the parameters $a_1 = 1.2$, $a_3 = 1.1$, $V_{21} = 3.2$ and $V_{43} = 0.8$.

part (b). How the hydrodynamically induced repulsive or attractive dumbbell motion depends on the parameters, describing the system's asymmetry, is illustrated in terms of diagrams for representative sets of parameters in figures 10–12.

In figure 10, areas of dumbbell attraction and repulsion are shown as a function of the two coupling parameters V_{21} and V_{43} for the fixed parameters, $a_1 = 1.2$ and $a_3 = 1.1$, corresponding to unequal dumbbell shapes. For combinations of the two couplings along the solid lines in figure 10, the bead asymmetries of the dumbbells are compensated for by the difference between V_{21} and V_{43} , so that the distance $D(t)$ is constant in the mean. If one coupling parameter is much larger than the other one ($V_{21} \gg V_{43}$ or $V_{43} \gg V_{21}$) the dumbbells attract each other. Between those two regimes there is a range of parameters for which the dumbbells repel each other. For increasing coupling constants the repulsive area widens.

In figure 11, the regions of dumbbell attraction and repulsion are shown as functions of the two bead radii a_1 and a_3 for fixed coupling constants, $V_{21} = 1.2$ and $V_{43} = 1.0$. For these

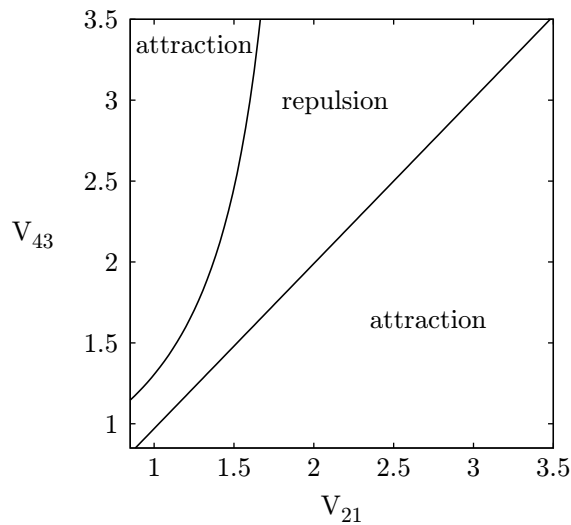


Figure 10. Ranges of dumbbell attraction and repulsion are shown as a function of the coupling constants V_{21} and V_{43} for slightly differing dumbbell asymmetries: $a_1 = 1.2$ and $a_3 = 1.1$.

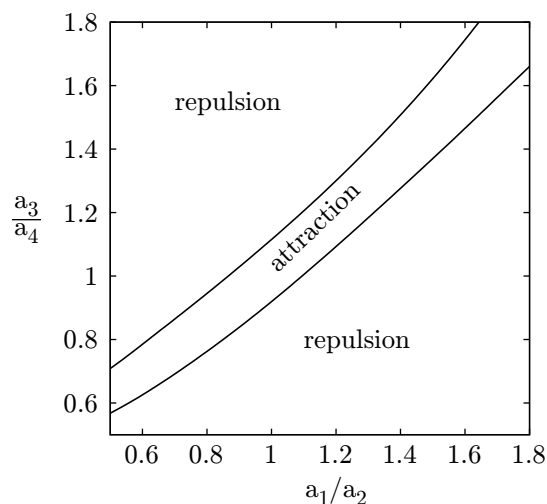


Figure 11. Ranges of dumbbell attraction and repulsion are shown as functions of the ratios of the bead radii a_1/a_2 and a_3/a_4 for unequal coupling parameters, $V_{21} = 1.2$ and $V_{43} = 1.0$.

parameters there is only a narrow domain, in which the dumbbells attract each other. In this area, the dumbbell asymmetries differ by only about 20–30%. The phase diagram in figure 11 also shows that for identical asymmetries of the two dumbbells, $a_1 = a_3$, one may have either dumbbell repulsion, as in the case $a_1 = a_3 = 0.6$, or attraction, as in the case $a_1 = a_3 = 1.8$.

In figure 12 the coupling $V_{43} = 1.0$ and the asymmetry $a_3/a_4 = 1.1$ of one of the dumbbells were fixed, whereas the asymmetry a_1/a_2 , as well as the coupling parameter V_{21} , is varied. For a symmetric or slightly asymmetric dumbbell, i.e. $a_1/a_2 \approx 1$, there is always attraction, but for stronger asymmetries there are also regions where the two dumbbells repel each other. Even

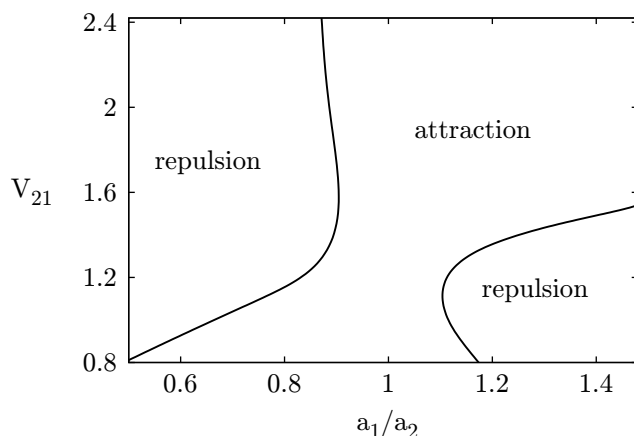


Figure 12. Ranges of dumbbell attraction and repulsion are shown as a function of the coupling strength V_{21} and the bead radius a_1 . The other parameters are $V_{43} = 1.0$ and $a_3 = 1.1$.

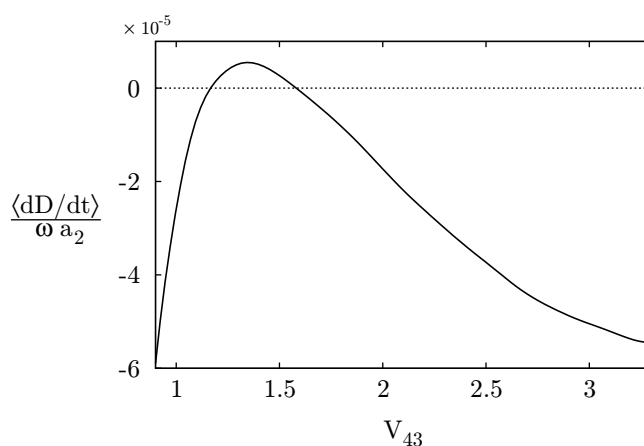


Figure 13. The mean relative velocity between the dumbbells is shown as a function of the coupling strength V_{43} for the same parameter set, as in figure 10 and the fixed value $V_{21} = 1.2$.

for equal couplings ($V_{21} = V_{43}$) one can find areas of dumbbell attraction as well as regions in which the dumbbells repel each other.

Away from the solid lines of vanishing attraction and repulsion in figure 10, 11 or 12 the modulus of the relative velocity between the dumbbells increases with the distance from these lines. This is demonstrated in figure 13, where the mean relative velocity between the dumbbells is shown as a function of the coupling V_{43} . In this figure, the same parameter set as in figure 10 was used and $V_{21} = 1.2$ was fixed. In this case the transitions from attraction to repulsion and back occur at the values $V_{43} \approx 1.17$ and $V_{43} \approx 1.59$ and there is only a small range of values of V_{43} for which the dumbbells repel each other.

Is there a simple mechanism by which the attractive or repulsive behavior can be explained? As shown before, the broken time-reversal symmetry of $D(t)$ is necessary for the non-reciprocal motion of the dumbbells to occur. Furthermore, for some parameter sets, the phase shift $\Delta\phi$

between the dumbbells, as well as its modulation amplitude, has a minimum in the repulsive regime. However, this depends very much on the parameters being used. For other parameter sets, $\Delta\phi$ takes its maximum value in the range in which the dumbbells repel each other. For a third class of parameter sets, there is no obvious correlation between the phase shift and the fact that the dumbbells behave in an attractive or a repulsive way. All in all, the mechanism leading to dumbbell attraction or repulsion is a complex interplay between the applied torques resulting from the coupling parameters and the drag forces, which depend on the bead radii and thus on the asymmetries of the dumbbells.

4. Conclusions and discussion

Hydrodynamic interactions between two rotating asymmetric dumbbells in a fluid at a low Reynolds number were investigated. We found either a temporally averaged attraction or repulsion between the dumbbells if they had different shapes and/or their couplings to the driving field differed. Differences in shape and/or coupling break the time-reversal symmetry and are hence a pre-condition for attraction or repulsion. No generic rule could be identified concerning whether a specific form of symmetry breaking leads to dumbbell attraction or repulsion. We presented phase diagrams separating parameter regions of attraction from regions of repulsion.

We suggest experiments where anisotropic birefringent particles are rotated by circularly polarized light, similar to recent experiments [28, 29], in order to explore the hydrodynamic attraction and repulsion between rotating small particles. In such experiments the torque on an anisotropic particle may easily be tuned by varying the laser power. Different torques may also be applied to the particles by using different shapes or materials for the particles. A spatially varying power of the circularly polarized light can also cause different torques on neighboring particles.

Dumbbells or anisotropic particles can also be constructed from super-paramagnetic particles, which can be rotated using a magnetic field. In this case, the magnetic dipole–dipole interactions have to be taken into account. Magic angle spinning may suppress the magnetic dipole or multipole interactions [26] such that the hydrodynamic interactions dominate.

Recently, synchronization and phase-locking effects have been reported in related systems [33, 34]. Both phenomena have not been observed for our model. This may be due to the fact that in our system the dumbbells can perform free translatory motion, whereas the locations of the objects in the cited works are more or less fixed.

If the hydrodynamic interactions of an assembly of asymmetric objects are investigated, collective dynamics such as chaotic motion can be expected. Our findings might find applications in designing an efficient way to micromix a fluid or to separate particles on the small scale. It might also be useful for studies on the collective assembly of micro-swimmers.

Acknowledgments

We thank J Bammert for instructive discussions. This work was supported by the German Science Foundation through the priority program on micro- and nanofluidics SPP 1164 and the research group FOR 608.

References

- [1] Taylor G I 1951 *Proc. R. Soc. A* **209** 447
- [2] Happel J and Brenner H 1991 *Low Reynolds Number Hydrodynamics* (Dordrecht: Kluwer)
- [3] Berg H C and Anderson R A 1973 *Nature* **245** 380
- [4] Purcell E M 1977 *Am. J. Phys.* **45** 3
- [5] Pedley T J and Kessler J O 1992 *Ann. Rev. Fluid Mech.* **24** 313
- [6] Stone H A and Kim S 2001 *AIChE J.* **47** 1250
- [7] Campbell C J and Grzybowski B A 2004 *Phil. Trans. R. Soc. A* **362** 1069
- [8] Ishikawa T, Simmonds M P and Pedley T J 2006 *J. Fluid Mech.* **568** 119
- [9] Lauga E and Powers T R 2009 *Rep. Prog. Phys.* **72** 096601
- [10] Becker L E, Koehler S A and Stone H A 2003 *J. Fluid Mech.* **490** 15
- [11] Dreyfus R, Baudry J, Roper M L, Fermigier M, Stone H A and Bibette J 2005 *Nature* **437** 862
- [12] Avron J E, Kenneth O and Oaknin D H 2005 *New J. Phys.* **7** 234
- [13] Dreyfus R, Baudry J and Stone H A 2005 *Eur. Phys. J. B* **47** 161
- [14] Cantat I and Misbah C 1999 *Phys. Rev. Lett.* **83** 880
- [15] Seifert U 1999 *Phys. Rev. Lett.* **83** 876
- [16] Abkarian M, Lartigue C and Viallat A 2002 *Phys. Rev. Lett.* **88** 068102
- [17] Lutz C, Reichert M, Stark H and Bechinger C 2006 *Europhys. Lett.* **74** 719
- [18] Holzer L and Zimmermann W 2006 *Phys. Rev. E* **73** 060801
- [19] Leal L G 1980 *Ann. Rev. Fluid Mech.* **12** 435
- [20] Kaoui B, Ristow G H, Cantat I, Misbah C and Zimmermann W 2008 *Phys. Rev. E* **77** 021903
- [21] Bammert J *et al* 2009 Reversal of cross-stream line migration in Poiseuille flow unpublished
- [22] Meiners J C and Quake S R 1999 *Phys. Rev. Lett.* **82** 2211
- [23] Ziehl A, Bammert J, Holzer L, Wagner C and Zimmermann W 2009 *Phys. Rev. Lett.* **103** 230602
- [24] Grzybowski B A, Jiang X, Stone H A and Whitesides G M 2000 *Phys. Rev. E* **64** 011603
- [25] Tierno P, Muruganathan R and Fischer T M 2007 *Phys. Rev. Lett.* **98** 028301
- [26] Tierno P, Schreiber S, Zimmermann W and Fischer T M 2009 *J. Am. Chem. Soc.* **131** 5366
- [27] Kim M and Powers T R 2004 *Phys. Rev. E* **69** 061910
- [28] Cheng Z, Chaikin P M and Mason T G 2002 *Phys. Rev. Lett.* **89** 108303
- [29] Bishop A I, Nieminen T A, Heckenberg N R and Rubinsztein-Dunlop H 2004 *Phys. Rev. Lett.* **92** 198104
- [30] Abragam A 1961 *Principles of Nuclear Magnetism* (Oxford: Oxford University Press)
- [31] Rotne J and Prager S 1969 *J. Chem. Phys.* **50** 11
- [32] Jeffrey D J and Onishi Y 1984 *J. Fluid Mech.* **139** 261
- [33] Niedermayer T, Eckhardt B and Lenz P 2008 *Chaos* **18** 037128
- [34] Qian B, Jiang H, Gagnon D A, Breuer K S and Powers T R 2009 *Phys. Rev. E* **80** 061919